Alfvénic Velocity Spikes and Rotational Flows in the Near-Sun Solar Wind

Justin C. Kasper, Stuart D. Bale, John W. Belcher, Matthieu Berthomier, Anthony W. Case, Benjamin D. G. Chandran, D.W. Curtis, D. Gallagher, S.P. Gary, L. Golub, et al.

Alfvénic velocity spikes and rotational flows in the near-Sun solar wind

Alfvénic Velocity Spikes and Rotational Flows in the Near-Sun Solar Wind

J. C. Kasper[1,2*], S. D. Bale[3,4,5], J. W. Belcher[6], M. Berthomier[7], A. W. Case[2], B. D. G. Chandran[8,9], D. W. Curtis[4], D. Gallagher[10], S. P. Gary[11], L. Golub[2], J. S. Halekas[12], G. C. Ho[13], T. S. Horbury[5], Q. Hu[14], J. Huang[1], K. G. Klein[15,16], K. E. Korreck[2], D. E. Larson[4], R. Livi[4], B. Maruca[17,18], B. Lavraud[19], P. Louarn[19], M. Maksimovic[20], M. Martinovic[15], D. McGinnis[12], N. V. Pogorelov[14], J. D. Richardson[6], R. M. Skoug[11], J. T. Steinberg[11], M. L. Stevens[2], A. Szabo[19], M. Velli[21], P. L. Whittlesey[4], K. H. Wright[25], G. P. Zank[14], R. J. MacDowall[19], D. J. McComas[22], R. L. McNutt, Jr.[13], M. Pulupa[4], N. E. Raouafi[13], and N. A. Schwadron[8,9]

[1]Climate and Space Sciences and Engineering, University of Michigan, Ann Arbor, MI 48109, USA
[2]Smithsonian Astrophysical Observatory, Cambridge, MA 02138, USA
[3]Physics Department, University of California, Berkeley, CA 94720-7300, USA
[4]Space Sciences Laboratory, University of California, Berkeley, CA 94720-7450, USA
[5]The Blackett Laboratory, Imperial College London, London, SW7 2AZ, UK
[6]Kavli Center for Astrophysics and Space Sciences, Massachusetts Institute of Technology, 77 Massachusetts Avenue Cambridge, MA 02139-4307, USA
[7]Laboratoire de Physique des Plasmas, CNRS, Sorbonne Universite, Ecole Polytechnique, Observatoire de Paris, Universite Paris-Saclay, Paris, 75005, France
[8]Department of Physics and Astronomy, University of New Hampshire, Durham, NH 03824, USA
[9]Space Science Center, University of New Hampshire, Durham, NH 03824, USA
[10]Heliophysics and Planetary Science Branch ST13, Marshall Space Flight Center, Huntsville, AL 35812, USA
[11]Los Alamos National Laboratory P.O. Box 1663 Los Alamos, NM 87545, USA
[12]Department of Physics and Astronomy, University of Iowa, IA 52242, USA
[13]Johns Hopkins University Applied Physics Laboratory 11100 Johns Hopkins Road, Laurel, MD 20723-6099, USA
[14]Department of Space Science and Center for Space Plasma and Aeronomic Research, University of Alabama in Huntsville, Huntsville, AL 35805, USA
[15]Lunar and Planetary Laboratory, University of Arizona, Tucson, AZ 85721, USA
[16]Department of Planetary Sciences, University of Arizona, Tucson, AZ 85719, USA
[17]Department of Physics and Astronomy, University of Delaware, Newark, DE 19716, USA
[18]Bartol Research Institute, University of Delaware, Newark, DE 19716, USA
[19]NASA/Goddard Space Flight Center, Greenbelt, MD 20771, USA
[20]LESIA, Observatoire de Paris, Universite PSL, CNRS, Sorbonne Universite, Universite de Paris, 5 place Jules Janssen, 92195 Meudon, France
[21]Department of Earth, Planetary & Space Sciences, University of California, Los Angeles CA 90095, USA
[22]Department of Astrophysical Sciences, Princeton University, Princeton, NJ 08544, USA
[24]Institut de Recherche en Astrophysique et Planétologie, CNRS, UPS, CNES, Université de Toulouse, Toulouse, France
[25]Universities Space Research Association, Science and Technology Institute, Huntsville AL 35805, USA
[*]jckasper@umich.edu

ABSTRACT

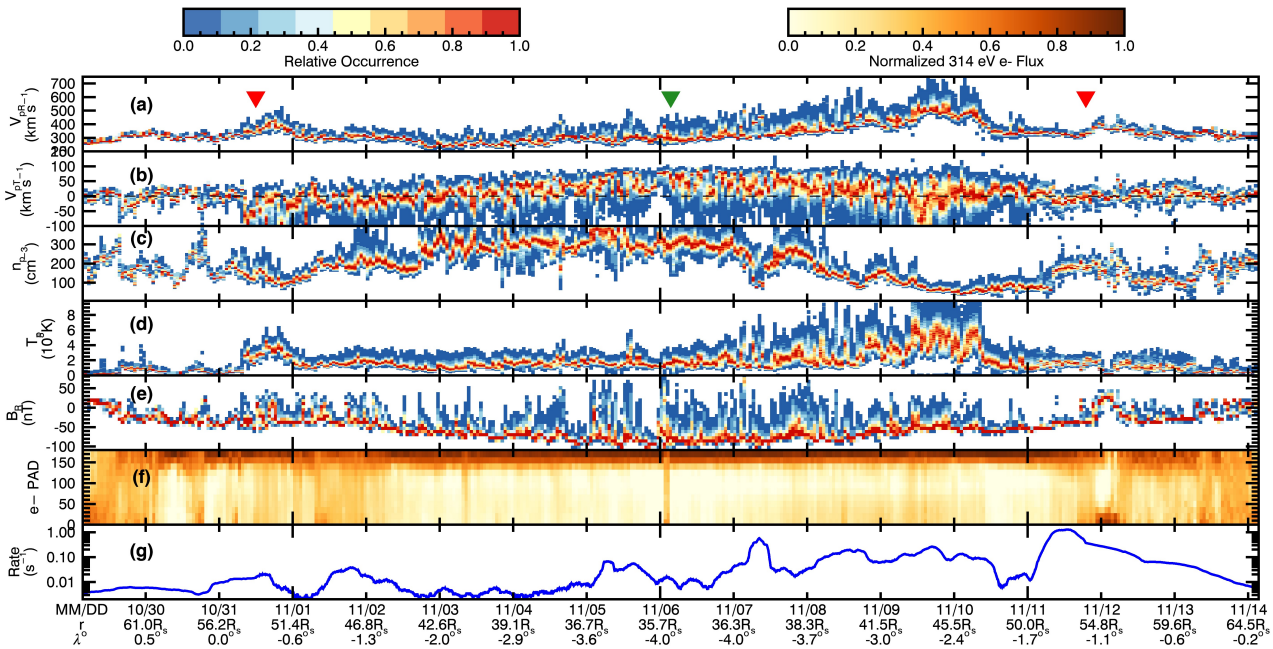

Figure 1. An overview of the first encounter with the Sun by Parker Solar Probe. (a) relative occurrence rate of proton radial speed V_{pR} in one hour intervals. Red triangles are the start and end of the high-rate data collection below $54R_S$ and the green triangle indicates perihelion at $35.7R_s$. (b) same for transverse component V_{pT} of proton velocity in solar equatorial plane, (c) proton number density n_p, (d) proton temperature T_p, (e) radial component of magnetic field B_R, (f) electron pitch-angle distribution, and (g) $20-200$ keV proton rate. The date, distance r, and latitude λ relative to the solar equator are indicated at daily intervals.

The prediction of a supersonic solar wind[1] was first confirmed by spacecraft near Earth[2,3] and later by spacecraft at heliocentric distances r as small as 62 solar radii (R_S)[4]. These missions showed that plasma accelerates as it emerges from the corona, aided by unidentified processes that transport energy outward from the Sun before depositing it in the wind. Alfvénic fluctuations are a promising candidate for such a process because they are seen in the corona and solar wind and contain significant energy[5–7]. Magnetic tension forces the corona to co-rotate with the Sun, but to date any residual rotation reported far from the Sun has been much smaller than the amplitude of waves and deflections from interacting wind streams[8]. Here we report observations of solar-wind plasma at $r \simeq 35R_S$[9–11], well inside the radius at which stream interactions become important. We find that the Alfvén waves organize into structured velocity spikes up to minutes long that are associated with propagating S-like bends in the magnetic-field lines. We detect an increasing azimuthal flow velocity of the solar wind around the Sun, peaking at $35-50\ km\ s^{-1}$, significantly above the amplitude of waves. These flows exceed classical predictions of a few $km\ s^{-1}$, challenging models of circulation in the corona and calling into question our understanding of how stars lose angular momentum and spin down as they age[12–14].

Parker Solar Probe (PSP) launched in August 2018 on a Delta IV Heavy rocket. The high energy of the launch combined with a gravitational assist from Venus in September 2018, placed PSP into an eccentric orbit with a period of 147 days and a perihelion at $r = 35.7R_S$, nearly a factor of two closer to the Sun than any previous mission[4]. This letter makes use of observations collected by instruments on the spacecraft during the first two encounters with the Sun in November 2018 and April 2019. While the instruments collect observations at a low rate far from the Sun, the primary science collection at high rate occurs during the encounter phase of each orbit at $r < 54R_S$ (0.25 au). Encounter one (E1) lasted from 31 October to 12 November 2018, with the first perihelion occurring at 03:27 UT on 6 November. During these two encounters the longitude of PSP relative to the rotating surface of the Sun barely changed; PSP essentially dove down into, and then rose straight up from, a single narrow region above the Sun. E1 and E2 data thus describe a handful of specific solar-wind streams.

Nearly two million thermal energy distribution functions of the solar-wind protons were recorded during E1, and more than three times that during E2 (Fig. 1, Extended Data Figure 1). From these distribution functions solar wind proton bulk properties such as velocity, density, and temperature are derived. Within any hour interval, the distribution of radial solar-wind speed

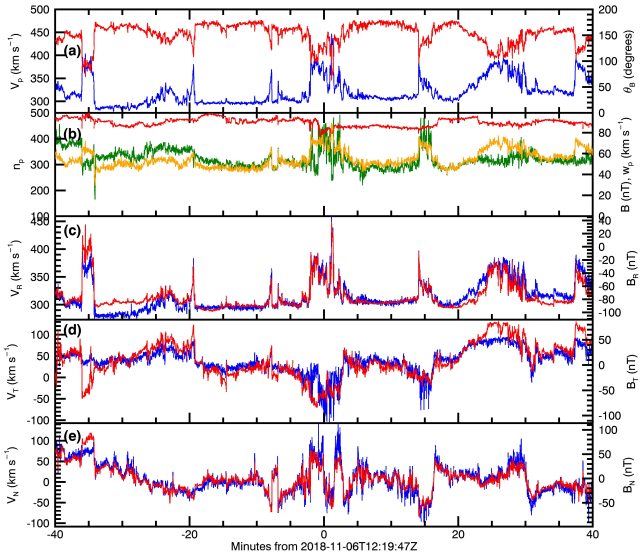

Figure 2. Solar wind fluctuations near closest approach. Near-Sun fluctuations meet Alfvénic criteria, but are organized into structures and contain density enhancements. (a) magnitude of V_{pR} (blue) and angle θ_{BR} of B from radial outwards, (b) magnitudes of n_p (green), B (red), and proton thermal speed w_p (yellow); (c-e) variation of each vector component of velocity (blue) and magnetic field (red) in the R, T, and N directions. There is a baseline solar wind speed with $\approx 300 km/s$ and jets where V_p jumps by $\approx 100 km/s$. The fluctuations are highly Alfvénic, with equal energy in field and flow, but organized into structures instead of randomly distributed, and there is evidence of compressions.

V_{pR} was strongly peaked at a minimum value, with a one-sided tail extending to larger V_{pR}. V_{pR} reached its minimum value of 200 km/s about a quarter of the way though E1 and then steadily rose to about 600 km/s. Numerical simulations and simple extrapolations of the observed photospheric magnetic field suggest that PSP spent all of E1 south of the global heliospheric current sheet (HCS), in a region with inward magnetic polarity ($B_R < 0$)[15]. Near the start and end of E1 PSP sampled slow wind from near the HCS. Closer to the Sun PSP observed first very slow wind and then fast wind, both of which are thought to emerge from a low-latitude coronal hole[15]. Below 40 R_S, V_{pT} has a net positive value, which peaks at closest approach. This flow may be the long-sought signature of plasma co-rotation in the corona. The density peaks in the slowest wind, at a value of approximately 400 cm^{-3}, about 50 times higher than typical values at 1 au, as expected from mass conservation and spherical expansion. The proton temperature T_p and V_{pR} remain positively correlated[16]. At perihelion the protons are ≈ 4 times hotter than protons with similar V_{pR} at 1 au, consistent with radial scalings reported from earlier missions[4]. The radial component of the magnetic field, B_R, increases in magnitude with proximity to the Sun but unexpectedly changes sign many times. The pitch-angle (θ) distribution (PAD) for electrons, or the number of electrons at a given energy as a function of their angle relative to B, is a valuable diagnostic of these changes in the direction of B. Here we show the PAD in a 22-eV-wide energy channel centered on 314 eV, well above the electron thermal energy. The sharp peak near 180° corresponds to the *strahl*, a beam of super-thermal electrons that travel away from the Sun along magnetic-field lines. Near the Sun strahl evolves towards small $\sin\theta$ because of magnetic-moment conservation[17]. If the reversals in B_R seen by PSP result from PSP's crossing between open field lines (connected to the Sun at only one end) with different signs of B_R back at the Sun, then the strahl would flip between 180° and 0° each time B_R changed sign. Instead, every time B_R flips, the strahl maintains its 180° orientation, clearly indicating that the reversals in B_R are due to S-like bends in the magnetic-field lines (Extended Data Figure 2). Closed field lines with both ends connected to the Sun and strahl traveling both parallel and anti-parallel to $\boldsymbol{B}$ are seen during the arrival of a coronal mass ejection on 12 November, following an enhancement in energetic particles[18].

Fig. 2 shows a timeseries of 80 minutes of observations several hours after perihelion illustrating typical velocity and magnetic-field fluctuations. About half the time B points radially inward towards the Sun and V sits at a relatively constant $300 km/s$. The remaining time includes seven distinct intervals in which B rotates away from its radial-inwards orientation

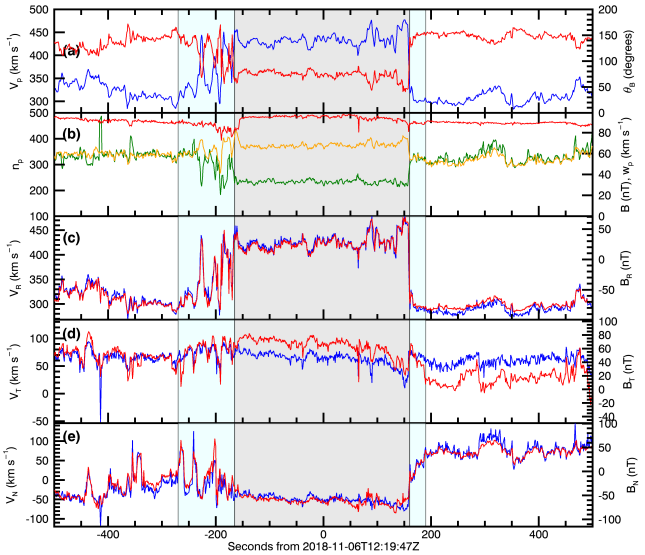

Figure 3. A closer look at a velocity spike. The same formatting is used as in Figure 2, but focused on a single 1,000 second interval. The left blue region indicates the 105 s period when PSP moved from the ambient plasma into the spike. The central core of the spike is indicated by the grey region and lasted for 325s, characterized by steady but disturbed flow and field with a large rotation in B to $\theta_B \sim 70°$, a jump in flow to 343 $km\ s^{-1}$. Return from the core spike into ambient solar wind is marked by the second blue region and took 30s.

and $V_{\rm pR}$ simultaneously jumps and V also rotates, linking the one-sided tail in V_{pR} and the reversals in polarity seen in the E1 overview. These jumps in flow associated with rotations in B and V are similar to one-sided Alfvénic structures first seen farther from the Sun[6,7]. The spikes seen by PSP are different in that they have larger amplitudes and are often associated with an increase in density, n_p, indicating that the spikes have a non-Alfvénic component. The correlated variations in the components of B and V, their relative amplitudes, and the constant value of $|B|$ are consistent with large-amplitude, spherically polarized Alfvén waves propagating through the plasma in the anti-Sunward direction, similar to earlier observations[5,19]. We can classify this wind stream (and indeed much of E1) as Alfvénic slow solar wind[20].

About 1,000 long-duration ($>$ 10 s) and isolated velocity spikes with large rotations in B were identified in E1. (About half as many were seen in E2.) Often the spikes can be separated chronologically into a core region with plasma conditions that are very different from the ambient solar wind but relatively constant, a comparatively short transition region on one side of the core, and a longer transition region on the other side containing large-amplitude fluctuations (See Fig. 3). During the 105s transition at the beginning of this spike the flow underwent seven large oscillations of amplitude 150kms^{-1}, possibly resulting from Kelvin-Helmoltz instability.

Equally unexpected as the spikes and B_R reversals are the large-amplitude and sustained positive rotational velocities seen below 40R_s for E1 and 50R_S for E2 (Fig. 4). Net rotation has been reported farther from the Sun, but it was on the same order as instrument error and much smaller than the standard deviation in flow due to fluctuations and stream interactions[8,21]. Here V_{pT} rises to 35 $km\ s^{-1}$ (E1) and 50 $km\ s^{-1}$ (E2). This is much greater than the variance from fluctuations including the velocity spikes, there is no evidence of stream interactions, and the values are much greater than the precision in averaged flows of less than 0.5 $km\ s^{-1}$ and an absolute error in flow due to a pointing error of less than 3 $km\ s^{-1}$ (See Methods). These are the first in situ observations of net rotational flow in the solar wind significantly above fluctuations and uncertainty.

Some level of rotational flow has always been expected in the solar wind near the Sun, as magnetic tension in the corona should force the plasma to rotate as the Sun spins. However, the large rotational velocities measured greatly exceed the value in the axisymmetric Weber-Davis model[13], posing a major challenge to our understanding of the dynamics of the near-Sun solar wind. Determining the origin of these tangential flows will be essential for understanding how the Sun loses angular momentum and spins down as it ages[12,14,22]. Further studies of the angular momentum should include magnetic fields, waves,

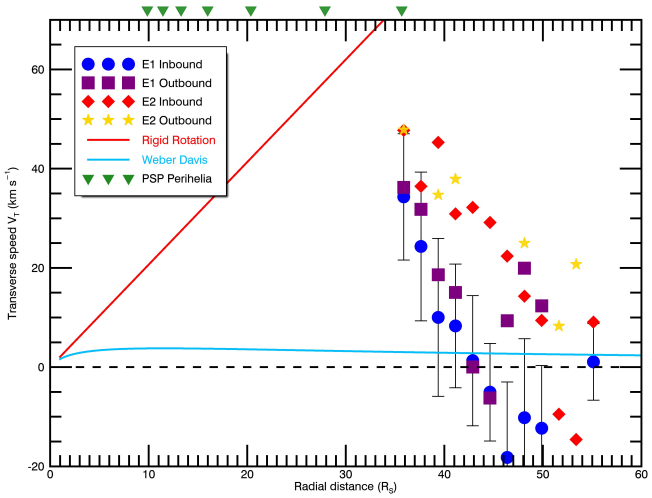

Figure 4. Large circulation of solar wind seen near Sun. Averaged rotational flow, V_{pT}, over $1.75R_S$ intervals during E1 (inbound in blue with error bars indicating standard deviation representative of all observations, outbound in purple) and E2 (inbound in red, outbound in yellow) as a function of radial distance. Each symbol is an average over at least 10,000 observations and the values closest to perihelion are averaged over 60,000-230,000 observations. Error bars for E1 inbound show one s.d. of the individual observations and are representative of the variation for the other 3 phases. The uncertainty in the mean of V_{pT} is much smaller than the symbols. Current and upcoming perihelia are shown with green triangles. Lines indicate no rotation (dashed), rigid co-rotation everywhere (red), and the axisymmetric Weber-Davis model (blue).

and other ions. Future PSP orbits will clarify the extent to which these large rotational flows characterize other solar-wind streams. These orbits will also provide critical additional diagnostics of the state of the plasma, including turbulence, velocity spikes, temperature anisotropy, and particle velocity-distribution functions, at heliocentric distances as small as $9.86R_S$.

References

1. Parker, E. N. Dynamics of the Interplanetary Gas and Magnetic Fields. *Astrophys. J.* **128**, 664–676 (1958).
2. Gringauz, K. I., Bezrokikh, V. V., Ozerov, V. D. & Rybchinskii, R. E. A Study of the Interplanetary Ionized Gas, High-Energy Electrons and Corpuscular Radiation from the Sun by Means of the Three-Electrode Trap for Charged Particles on the Second Soviet Cosmic Rocket. *Soviet Physics Doklady* **5**, 361–364 (1960).
3. Bonetti, A., Bridge, H. S., Lazarus, A. J., Rossi, B. & Scherb, F. Explorer 10 Plasma Measurements. *J. Geophys. Res.* **68**, 4017–4063 (1963).
4. Marsch, E. *et al.* Solar wind protons - Three-dimensional velocity distributions and derived plasma parameters measured between 0.3 and 1 AU. *J. Geophys. Res.* **87**, 52–72 (1982).
5. Belcher, J. W. & Davis, J., Leverett. Large-amplitude Alfvén waves in the interplanetary medium, 2. *J. Geophys. Res.* **76**, 3534–3563 (1971).
6. Gosling, J. T., McComas, D. J., Roberts, D. A. & Skoug, R. M. A One-Sided Aspect of Alfvenic Fluctuations in the Solar Wind. *Astrophys. J. Lett.* **695**, L213–L216 (2009).
7. Horbury, T. S., Matteini, L. & Stansby, D. Short, large-amplitude speed enhancements in the near-Sunfast solar wind. *Mon. Not. Roy. Astron. Soc.* **478**, 1980–1986 (2018).
8. Pizzo, V. *et al.* Determination of the solar wind angular momentum flux from the HELIOS data - an observational test of the Weber and Davis theory. *apj* **271**, 335–354 (1983).
9. Fox, N. J. *et al.* The Solar Probe Plus Mission: Humanity's First Visit to Our Star. *Space Sci. Rev.* **204**, 7–48 (2016).
10. Kasper, J. C. *et al.* Solar Wind Electrons Alphas and Protons (SWEAP) Investigation: Design of the Solar Wind and Coronal Plasma Instrument Suite for Solar Probe Plus. *Space Sci. Rev.* **204**, 131–186 (2016).
11. Bale, S. D. *et al.* The FIELDS Instrument Suite for Solar Probe Plus. Measuring the Coronal Plasma and Magnetic Field, Plasma Waves and Turbulence, and Radio Signatures of Solar Transients. *Space Sci. Rev.* **204**, 49–82 (2016).

12. Schatzman, E. A theory of the role of magnetic activity during star formation. *Annales d'Astrophysique* **25**, 18–29 (1962).

13. Weber, E. J. & Davis, J., Leverett. The Angular Momentum of the Solar Wind. *Astrophys. J.* **148**, 217–227 (1967).

14. Finley, A. J., Matt, S. P. & See, V. The Effect of Magnetic Variability on Stellar Angular Momentum Loss. I. The Solar Wind Torque during Sunspot Cycles 23 and 24. *Astrophys. J.* **864**, 125 (2018).

15. Bale, S. D. *et al.* The magnetic structure and electrodynamics of the emerging solar wind. *Nature* (Submitted).

16. Elliott, H. A., Henney, C. J., McComas, D. J., Smith, C. W. & Vasquez, B. J. Temporal and radial variation of the solar wind temperature-speed relationship. *Journal Geophysical Research: Space Physics* **117** A09102 (2012).

17. Pilipp, W. G. *et al.* Characteristics of electron velocity distribution functions in the solar wind derived from the helios plasma experiment. *jgr* **92**, 1075–1092 (1987).

18. McComas, D. M. *et al.* Energetic Particle Environment near the Sun from Parker Solar Probe. *Nature* (Submitted).

19. Vasquez, B. J. & Hollweg, J. V. Formation of arc-shaped Alfvén waves and rotational discontinuities from oblique linearly polarized wave trains. *J. Geophys. Res.* **101**, 13527–13540 (1996).

20. Bruno, R. & Carbone, V. The Solar Wind as a Turbulence Laboratory. *Living Reviews Solar Physics* **10**, 2 (2013).

21. Richardson, I. G. Solar wind stream interaction regions throughout the heliosphere. *Living Reviews Solar Physics* **15**, 1 (2018).

22. Axford, W. I. The Solar Wind. *Solar Physics* **100**, 575–586 (1985).

Figure Legends

Figure 1: An overview of the first encounter with the Sun by Parker Solar Probe.

(a) relative occurrence rate of proton radial speed V_{pR} in one hour intervals. Red triangles are the start and end of the high-rate data collection below $54R_S$ and the green triangle indicates perihelion at $35.7R_s$. (b) same for transverse component V_{pT} of proton velocity in solar equatorial plane, (c) proton number density n_p, (d) proton temperature T_p, (e) radial component of magnetic field B_R, (f) electron pitch-angle distribution, and (g) $20-200$ keV proton rate. The date, distance r, and latitude λ relative to the solar equator are indicated at daily intervals.

Figure 2: Solar wind fluctuations near closest approach.

Near-Sun fluctuations meet Alfvénic criteria, but are organized into structures and contain density enhancements. (a) magnitude of V_{pR} (blue) and angle θ_{BR} of B from radial outwards, (b) magnitudes of n_p (green), B (red), and proton thermal speed w_p (yellow); (c-e) variation of each vector component of velocity (blue) and magnetic field (red) in the R, T, and N directions. There is a baseline solar wind speed with $\approx 300 km/s$ and jets where V_p jumps by $\approx 100 km/s$. The fluctuations are highly Alfvénic, with equal energy in field and flow, but organized into structures instead of randomly distributed, and there is evidence of compressions.

Figure 3: A closer look at a velocity spike.

The same formatting is used as in Figure 2, but focused on a single 1,000 second interval. The left blue region indicates the 105 s period when PSP moved from the ambient plasma into the spike. The central core of the spike is indicated by the grey region and lasted for $325s$, characterized by steady but disturbed flow and field with a large rotation in B to $\theta_B \sim 70^\circ$, a jump in flow to 343 $km\ s^{-1}$. Return from the core spike into ambient solar wind is marked by the second blue region and took $30s$.

Figure 4: Large circulation of solar wind seen near Sun.

Averaged rotational flow, V_{pT}, over $1.75R_S$ intervals during E1 (inbound in blue with error bars indicating standard deviation representative of all observations, outbound in purple) and E2 (inbound in red, outbound in yellow) as a function of radial distance. Each symbol is an average over at least 10,000 observations and the values closest to perihelion are averaged over 60,000-230,000 observations. Error bars for E1 inbound show one s.d. of the individual observations and are representative of the variation for the other 3 phases. The uncertainty in the mean of V_{pT} is much smaller than the symbols. Current and upcoming perihelia are shown with green triangles. Lines indicate no rotation (dashed), rigid co-rotation everywhere (red), and the axisymmetric Weber-Davis model (blue).

Extended Data Figure 1: An overview of the second encounter with the Sun by Parker Solar Probe.

In the same format as Fig. 1. Spikes in the velocity are again seen coincident with the magnetic field reversals, but the jump in speed is smaller, likely because the Alfvén speed was slower in E2 than E1. The density at perihelion is substantially lower.

Extended Data Figure 2: Schematic of an "S-shaped" magnetic structure creating a field reversal, heat flux reversal, and spike in velocity.

This figure illustrates the possible geometry of an "S-shaped" propagating Alfvénic disturbance (gray box) and how it would appear to the spacecraft (black square) as it flew through the spike on the green trajectory. The light lines with arrows indicate the configuration of the magnetic field, with all field lines ultimately pointed back to the Sun. Arrows at each black square indicate the vector velocity (blue), electron strahl (orange), and magnetic field (red) seen by the spacecraft. If this was a purely Alfvénic structure then the spike would move away from the Sun anti-parallel to B at the local Alfvén speed, C_A. In the frame of the spike the shape of the structure would be static, with plasma flowing in along field lines on the upper left and through the spike, emerging at the lower right, always flowing at C_A. In the frame of the spacecraft, the constant flow along field lines in the propagating spike frame would translate into a radial increase of V by C_A when B was perpendicular to R, and a maximum jump of $2C_A$ when B was completely inverted. Since the heat flux escapes away from the Sun, it would rotate so as to always be anti-parallel to B and appear to be flowing back to the Sun at the center of this disturbance.

Methods

Data Collection and Analysis The data presented in this letter were collected over the course of the first two encounters of the Sun by Parker Solar Probe in November 2018 and April 2019. This study makes use of all of the in situ instruments on the spacecraft. Thermal plasma properties are measured by the PSP SWEAP instrument suite[10], including the Solar Probe (SPC) Cup, SPAN electron, and SPAN ion plasma data. Magnetic field data from the outboard FIELDS magnetometer was also used[11,15], along with energetic particle rates as seen by $IS\odot IS$[18]. SPC measures the reduced distribution function of ionized hydrogen and helium and the two dimensional flow angles of the ions as a function of energy/charge. These measurements are performed at least once per second and typically more than four times per second throughout the encounter phase of each orbit (below 0.25 *au* or 54 R_s). This paper uses moments of the entire SPC proton distribution function to calculate a total effective proton velocity, density, and radial component of the temperature. While the SPAN ion sensor generally did not view the peak of the proton velocity distribution, the overlapping region seen by SPAN and SPC has been compared to confirm that there are no gross offsets in calibration or derived plasma properties such as velocity, but this technique will be more accurate when the solar wind flows into SPAN closer to the Sun. Observations of electrons with a center energy of 314 eV and width of 22 eV by the two SPAN electron sensors were combined, along with the FIELDS determination of the magnetic field direction, to create the electron pitch angle distributions.

All underlying data are being archived and will be available for download at the NASA Space Physics Data Facility in November 2019[23]. Additional SWEAP data and information are available at the SWEAP web page[24]. Data were analyzed and graphics developed in the Interactive Data Language (IDL).

Statistics The distributions of plasma properties in Fig. 1 and Extended Data Figure 1 were produced with one hour time resolution. During the encounters the time resolution of the plasma instrument ranged from slightly more than one measurement per second to more than four measurements per second, so each column in those panels represents the distribution of approximately 3,600-14,400 measurements. All error bars indicate one standard deviation (s.d.) of the measurements from the mean. At least 10,000 and generally more than 80,000 observations are used in calculating the mean transverse flow V_{pT} in Figure 4.

Estimates of Uncertainty The absolute accuracy of the Solar Probe Cup (SPC) ion measurements are summarized here. As verified in ground testing, the absolute accuracy for V_{pR} is less than 0.01% over a measurable range of approximately 119 km/s to 1065 km/s. The absolute accuracy in temperature is similarly negligible over a measurable range of approximately 7.3 kK to 21.1 MK (i.e. thermal speeds of 11 km/s to 600 km/s). Speeds and temperatures at the extremes of these ranges are subject to systematic considerations, but no such measurements have been presented here. The accuracy of the density measurement is determined by comparison with the plasma frequency as observed by FIELDS[11]. Thus the absolute accuracy of the SPC density measurement is estimated at $\approx 1\%$ and is no worse than 3%. The absolute accuracy for off-radial flow components are verified via spacecraft roll maneuvers about the SPC symmetry axis. For solar wind fluxes typical of the first two encounters, the uncertainty associated with this calibration corresponds to a typical absolute accuracy of $\approx$0.5 degrees. For 400 $km\ s^{-1}$ solar wind this corresponds to an expected error in V_{pT} of $3-4\ km\ s^{-1}$, which is much smaller than the net rotational flow observed.

Signatures of Alfvénic Fluctuations In discussing Fig. 2 we stated that the correlation of fluctuations in components of $\mathbf{B}$ and $\mathbf{V}$ were generally indicative of outward propagating Alfvén waves. Consider vector waves or fluctuations $\Delta\mathbf{V}$ and $\Delta\mathbf{B}$ superimposed on a steady background $\mathbf{B}_\circ$ and $\mathbf{V}_\circ$. In the long wavelength fluid magnetohydrodynamic (MHD) limit Alfvén waves propagate exactly parallel or anti-parallel to $\mathbf{B}_\circ$, are dispersionless and do not compress the plasma, and there is a simple linear relationship $\Delta\mathbf{B} = \pm D_A \Delta\mathbf{V}$, where $D_A = (n_p + 4n_\alpha)^{0.5}\Theta/21.8$ $(nT\ km^{-1}\ s)$, densities are in units of cm^{-3}, and $\Theta = (1-\beta_\parallel+\beta_\perp)^{-0.55}$. Here Θ is a correction for thermal pressure anisotropy where $\beta_\parallel$ is the ratio of parallel plasma pressure to magnetic pressure and $\beta_\perp$ is the ratio of perpendicular plasma pressure to $\mathbf{B}$. For this period we find that on average

$n_p = 220\ cm^{-3}$, $\beta_\parallel = 0.202$, and $\beta_\perp = 0.315$. SPC and SPAN were not configured optimally to measure the ionized helium abundance n_α, so assuming the typical range $0.5 < n_\alpha/n_p < 4.5\%$ we expect $D_A = 0.68 - 0.74\ (nT\ km^{-1}\ s)$. We find D_A for each of the RTN components to be $0.71, 1.09, 0.70\ (nT\ km^{-1}\ s)$, so the R and N components are exactly within the expected range and the fluctuations in the T direction are about 33% higher. It is common for the D_A to be different for each component of the velocity[5]. We then used the calculated value of D_A to rescale the range of the vector components of B so they should overlap with V if the fluctuations were purely Alfvénic. The sign of the relation between ΔB and ΔV is given by the sign of $-\mathbf{k}\cdot\mathbf{B}_\circ$, where k is the wavevector and gives the direction of propagation, and B is an average direction of the field over a long time scale. Since the ambient direction of the magnetic field outside the large amplitude fluctuations points towards the Sun and the correlations are overwhelmingly positive this means we are seeing outward waves.

Identification of velocity spikes. Isolated velocity spikes were identified by looking for all intervals in each encounter where the orientation of the magnetic field started in the quiet configuration pointed nearly towards the Sun, rotated more than 45° away from the quiet configuration for at least 10 seconds, and then returned back to the original direction. Candidate events were then examined manually to identify starting and ending times.

Methods References

23. NASA's Space Physics Data Facility https://spdf.gsfc.nasa.gov/.

24. The SWEAP Suite on Paker Solar Probe https://www.cfa.harvard.edu/sweap.

Acknowledgements

The SWEAP Investigation and this publication are supported by the PSP mission under NASA contract NNN06AA01C. The SWEAP team expresses its gratitude to the scientists, engineers, and administrators who have made this project a success, both within the SWEAP institutions and from NASA and the project team at JHU/APL. J.C.K. acknowledges support of the 2019 Summer School at the Center for Computational Astrophysics, Flatiron Institute. The Flatiron Institute is supported by the Simons Foundation. S.D.B. acknowledges the support of the Leverhulme Trust Visiting Professorship program. TH was supported by UK STFC ST/S0003641/1.

Author contributions statement

J.C.K. is the SWEAP Principal Investigator and led the data analysis and writing of this letter. S.D.B. is the FIELDS PI and a SWEAP Co-Investigator and provided the magnetic field observations. J.W.B. leads the US group where the solar wind Faraday cup was developed and provided guidance on identifying Alfvénic fluctuations. M.B. provided a pre-amplifier ASIC used within the SPAN electron instruments. A.W.C. is the Solar Probe Cup instrument scientist and ensured that the instrument met its performance requirements and was calibrated. B.D.G.C. contributed theoretical calculations and writing to the manuscript. D.W.C. D.G. was the institutional lead at NASA MSFC responsible for materials testing and calibration of SPC. S.P.G. provided recommendations on measurement requirements in order to detect instabilities. L.G. provided related solar observations and results. J. H. contributed to the analysis of the electron observations and to the manuscript. G.H. provided a time of flight ASIC to reduce the size and power of the SPAN ion instrument. T.H. participated in the analysis of the Alfvénic spikes. Q.H. identified magnetic flux ropes. K.G.K. contributed to writing the manuscript and provided warm plasma growth rate calculations. K.E.K. led the SWEAP Science Operations Center and coordinated observing plans between the instruments and the project. M.V. contributed to writing the manuscript and discussing the relationship between Alfvénic fluctuations and angular momentum. D.L. is the institutional lead at Berkeley responsible for the implementation of the SPAN instruments and the SWEAP Electronics Module suite-wide computer. R.L. is the SPAN ion instrument scientist. B.A.M. performed simulations of the fields of view of the SWEAP ion instruments and their probabilities of detecting the solar wind. B.L. identified flux ropes and other signatures of coronal mass ejections in the data. P.L. coordinated solar furnace testing of the Solar Probe Cup materials before launch. M.M. absolute calibration, quality of vdfs. N.P. Numerical simulations. J.D.R. FC design, radial variation. R.K.S. Electron PADs. J.T.S. field rotation causes. M.L.S. Overall data pipeline for SWEAP, SPC high level data products. A.S. estimated the location of the heliospheric current sheet. P.W. set up the SPC calibration at MSFC and then became SPAN electron instrument scientist at Berkeley . K.W. arranged the SPC calibration at MSFC. G.P.Z. leads the SWEAP theory team. R.J.M. leads the FIELDS fluxgate magnetometer. D.J.M. is the IS⊙IS PI. He provided the energetic particle data. R.M. Lead for the EPI-Lo energetic particle instrument. M.P. FIELDS SOC lead. N.R. PSP Project Scientist and reviewed jets and similar coronal transients. N.A.S. runs the IS⊙IS Science Operations Center. All authors participated in planning the observations and data collection, reviewed and discussed the observations, and read, provided feedback, and accepted the contents of the manuscript.

Author Information

Correspondence and requests for materials should be addressed to Justin Kasper (jckasper@umich.edu).

Extended Data – Online Supporting Materials

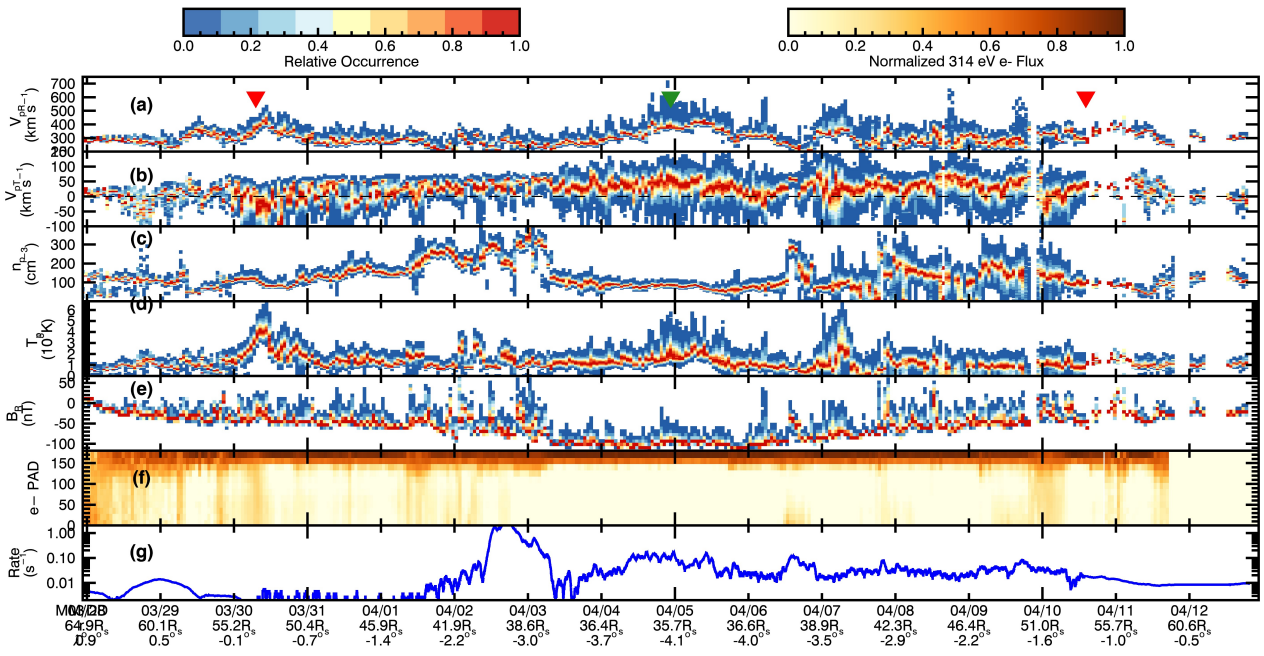

Extended Data Figure 1: An overview of the second encounter with the Sun by Parker Solar Probe.

In the same format as Fig. 1. Spikes in the velocity are again seen coincident with the magnetic field reversals. A net positive V_{pT} is seen at the second perihelion.

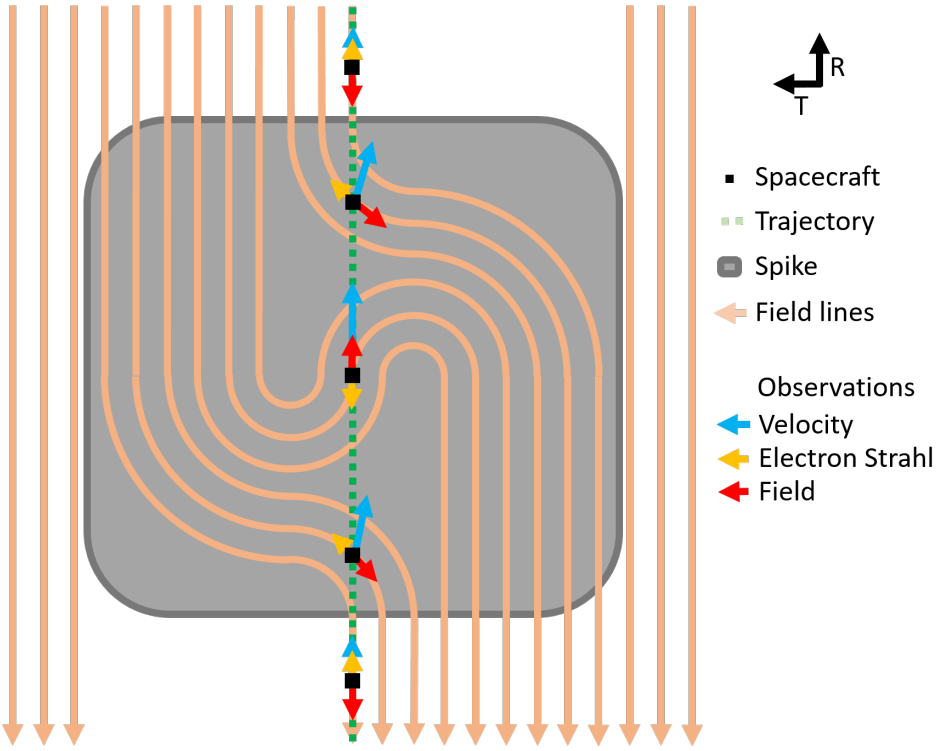

Extended Data Figure 2: Schematic of an "S-shaped" magnetic structure creating a field reversal, heat flux reversal, and spike in velocity.

This figure illustrates the possible geometry of an "S-shaped" propagating Alfvénic disturbance (gray box) and how it would appear to the spacecraft (black square) as it flew through the spike on the green trajectory. The light lines with arrows indicate the configuration of the magnetic field, with all field lines ultimately pointed back to the Sun. Arrows at each black square indicate the vector velocity (blue), electron strahl (orange), and magnetic field (red) seen by the spacecraft. If this was a purely Alfvénic structure then the spike would move away from the Sun anti-parallel to B at the local Alfvén speed, C_A. In the frame of the spike the shape of the structure would be static, with plasma flowing in along field lines on the upper left and through the spike, emerging at the lower right, always flowing at C_A. In the frame of the spacecraft, the constant flow along field lines in the propagating spike frame would translate into a radial increase of V by C_A when B was perpendicular to R, and a maximum jump of $2C_A$ when B was completely inverted. Since the heat flux flows away from the Sun, it would rotate so as to always be anti-parallel to B and appear to be flowing back to the Sun at the center of this disturbance.